PHYSICAL REVIEW B **77**, 224114 (2008)

Melting at dislocations and grain boundaries: A phase field crystal study

Joel Berry,[1] K. R. Elder,[2] and Martin Grant[1]
[1]*Physics Department, McGill University, Rutherford Building, 3600 rue University, Montréal, Québec, Canada H3A 2T8*
[2]*Department of Physics, Oakland University, Rochester, Michigan 48309-4487, USA*
(Received 24 January 2008; revised manuscript received 2 June 2008; published 26 June 2008)

Dislocation and grain-boundary melting are studied in three dimensions using the phase field crystal method. Isolated dislocations are found to melt radially outward from their core, as the localized excess elastic energy drives a power-law divergence in the melt radius. Dislocations within low angle to intermediate angle grain boundaries melt similarly until an angle-dependent first-order wetting transition occurs when neighboring melted regions coalesce. High angle boundaries are treated within a screening approximation, and issues related to ensembles, metastability, and grain size are discussed.

DOI: 10.1103/PhysRevB.77.224114 PACS number(s): 64.70.D−, 61.72.Bb, 61.72.Lk, 61.72.Mm

I. INTRODUCTION

Freezing and melting transitions do not exhibit the range of universal behavior associated with continuous phase transitions and largely for this reason have eluded a unified theoretical description. The nature of a given melting transition may depend sensitively on the details of the system and experiment and can involve many distinct processes both within and between multiple forms of excitations. For example, melting may occur abruptly and discontinuously at the melting temperature T_m, or it may initiate well below T_m at surfaces and/or internal defects and proceed up to T_m. This process of premelting has been studied extensively for surfaces[1,2] and is relatively well understood, but limited and inconsistent experimental evidence for melting at dislocations and grain boundaries leaves a number of issues unresolved.

A recent study of colloidal crystals has verified that premelting does occur at vacancies, dislocations, and grain boundaries and has provided measurements of the localized premelting behavior below T_m.[3] The conditions which determine whether premelting will occur continuously or discontinuously and whether the width of the premelted region diverges are not fully understood. Grain boundaries in Al have been found to liquify very near T_m, and the width of the melted layer appears to diverge.[4] Discontinuous jumps in grain-boundary diffusion coefficients,[5,6] mobility,[7] and shear resistance[8] have been found in other metals.

Theoretical studies have been based on either explicitly atomistic methods such as molecular dynamics[9,10] and Monte Carlo[11] or on continuum phase field models with uniform phases.[12–14] In this study, dislocation and grain-boundary melting are examined using the phase field crystal (PFC) method,[15] which extends the phase field approach to the level of atomistic resolution. This permits straightforward identification of stable equilibrium and metastable nonequilibrium atomic structures while inherently including crystal symmetry and orientation, elasticity/plasticity, and the individual dislocations which compose the grain boundaries. Our description will be most applicable to hard-sphere/colloidal systems and possibly simple metals.

The melting behavior of dislocation pairs and symmetric tilt grain boundaries of θ=4°, 8°, 16°, 24°, 32°, and 44° are examined numerically for a simple PFC model with bcc symmetry. Analytic results are derived for isolated dislocations and low θ boundaries by combining the PFC equations with continuum linear elasticity. A screening approximation is outlined for high angle boundaries, though somewhat surprisingly, the low θ description is found to remain reasonably accurate for high θ.

It has been shown[16] that the PFC free energy can be derived from the Ramakrishnan-Yussouff[17] free-energy functional of classical density-functional theory.[18] Here we give the final dimensionless form,

$$F = \int d\vec{r}\left[\frac{B_\ell}{2}n^2 + \frac{B_s}{2}n(2\nabla^2+\nabla^4)n - w\frac{n^3}{6} + \frac{n^4}{12}\right], \quad (1)$$

where the relations between model parameters and material parameters as well as their scaling can be found in previous work.[16] Here $n=(\rho-\bar{\rho})/\bar{\rho}$ is the scaled time-averaged number density, where ρ is the local-density variable and $\bar{\rho}$ is the average number density. B_ℓ and B_s are determined from the two-body correlation function of the liquid near freezing, and w is related to three-body correlations. Classical density-functional theory has been used to examine surface melting,[2,19] but not grain-boundary melting, presumably due to the complexity of the solid-solid interface and the more demanding system size requirements.

The dynamics are given in dimensionless form by

$$\frac{\partial n}{\partial t} = \nabla^2\frac{\delta F}{\delta n} + \eta, \quad (2)$$

where $\langle \eta(\vec{r}_1,t_1)\eta(\vec{r}_2,t_2)\rangle = M\nabla^2\delta(\vec{r}_1-\vec{r}_2)\delta(t_1-t_2)$. This form imposes a constant density and is consistent with the canonical ensemble. The stochastic term η sets the time scale for crossing free-energy barriers from dry to wet dislocation configurations locally when the wet state has lower free energy. It may also shift the "equilibrium" melting behavior to some degree since increasing the fluctuation amplitude M can increase the preferred size of a dislocation core or premelt radius and effectively lower the melting temperature. We have chosen to use a relatively small M in the simulations presented in this paper to minimize the effect of noise on the free energy yet still allow for barrier crossing.

 ©2008 The American Physical Society

A semi-implicit pseudospectral algorithm was used to solve Eq. (2) for systems containing either a single dislocation pair or a symmetric tilt grain-boundary pair with periodic boundary conditions. The parameters used were $\Delta x = 0.976\,031$, $\Delta t = 0.5$, $B_s = \sqrt{3}/3$, $w = 3^{1/4}/2$, and $M = 0.002$. These values were chosen because the model behavior has already been well characterized at this set in previous studies. The qualitative melting behavior appears to be relatively insensitive to the values used. A system size $V = (512\Delta x)^3 = (56a)^3$ was used for the dislocation pair and 4° grain-boundary pair, while $V = (256\Delta x)^3 = (28a)^3$ was used for all other grain-boundary pairs, where $a = 8.9237$ is the bcc lattice constant. Finite-size effects increase as θ decreases but were found to be small for all grain boundaries studied.

The temperature is taken to be proportional to $\Delta B \equiv B_\ell - B_s$ since the coefficient of the second-order term in F has leading temperature dependence and controls proximity to the critical point at $B_\ell = 0$ when $w = 0$. For $w \neq 0$ there is no critical point, and instead varying ΔB passes the system through a first-order liquid-solid transition at some $\Delta B_m = f(w)$.

II. SIMULATION RESULTS

The Gaussian width or mean-square displacement (D) of each localized density peak was monitored as the temperature ΔB was increased toward the melting point. The local crystallinity ϕ has been defined as

$$\phi(\vec{r}) = \frac{D(\vec{r}) - D_X}{D_L - D_X}, \tag{3}$$

where D_X is the equilibrium D of the crystal phase and D_L is that of the liquid phase. $\phi = 1/2$ specifies a liquid-solid interface.

The radius of the melted region around a dislocation core R_m was first measured in this manner for an edge dislocation pair as the temperature was raised toward the bulk melting temperature ΔB_m. The results are shown in Fig. 1, where the data are plotted as $(R_m + R_0)^{-2}$ vs ΔB to demonstrate that R_m is consistent with a $(\Delta B_m - \Delta B)^{-1/2}$ form which will be derived later. R_0 is an offset related to the finite size of the dislocation core at zero temperature. The fit to this form predicts a bulk melting temperature $\Delta B_m = 0.0270$ which is in good agreement with the directly measured value of $\Delta B_m = 0.0278$. The upper inset of Fig. 1 shows melting around an edge dislocation as $\Delta B \to \Delta B_m$.

Measurements of the radially and laterally averaged D due to dislocations and grain boundaries, respectively, are in qualitative agreement with those of Alsayed *et al.*[3] for colloidal crystals. We find that the decay can be fit adequately by either power law or exponential forms, with greater exponential character at large θ and greater power-law character at small θ.

Figure 2 shows the progression of melting at 8° and 44° grain boundaries. Low angle boundaries were found to first melt radially at each dislocation core until the melted regions of neighboring dislocations coalesce and a uniform wetting layer is formed along the boundary. In high angle boundaries individual dislocations cannot be distinguished and melting in this case was found to proceed by uniform disordering along the boundary rather than by local radial melting. Interfacial roughening due to thermal fluctuations was negligible in all simulations.

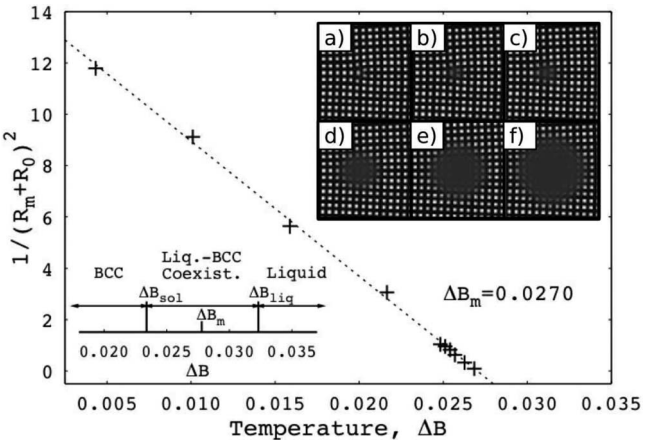

FIG. 1. Numerically measured local melt radius R_m around an edge dislocation in a bcc crystal as a function of temperature [units of lattice constant a, $\Delta B < 0.025$ values obtained by extrapolation of $\phi(\vec{r})$]. $R_0 = 0.2812a$ is the radius at $\Delta B = 0$, determined by best fit. Inset: cross-sectional images of the time-averaged number density field $n(x,y,z)$ from simulations at $\Delta B = 0.021\,65$, $0.025\,11$, $0.025\,69$, $0.026\,27$, $0.026\,56$, and $0.026\,85$ from (a)–(f), showing melting at a dislocation core.

The dependence of the width of the wetting layer (or the liquid volume fraction of the system) on ΔB is shown in the inset of Fig. 3 for various grain-boundary angles. In all cases the width remains narrow and the boundary relatively dry until above the solidus, at which point a discontinuous jump is observed at some characteristic wetting temperature ΔB_{wet}. The dependence of ΔB_{wet} on θ is shown in the main plot of Fig. 3. The fit lines will be discussed in the following, though the axes reveal that our predicted form will be $\Delta B_{\text{wet}} \propto \sin^2 \theta$.

III. LOCAL MELTING EQUATIONS

Based on these simulation results, we have developed a theory of dislocation-driven melting, which is easily extended to low angle grain boundaries. The low angle results are shown to remain accurate for all but the highest θ where the dislocation spacing d reaches the order of the Burger's vector b. A screening approximation for the spatial grain-boundary energy is found to be more applicable for very large θ, with a gradual crossover taking place between these two regimes. Our approach to low angle grain boundaries has similarities to the theory of Glicksman and Vold[20] for "heterophase" dislocations.

Isolated dislocations

According to continuum elasticity,[21] the radially averaged elastic energy density per length of dislocation line in a three-dimensional isotropic solid is $\bar{F}_{\text{el}} = \alpha\mu/R^2$, where μ is

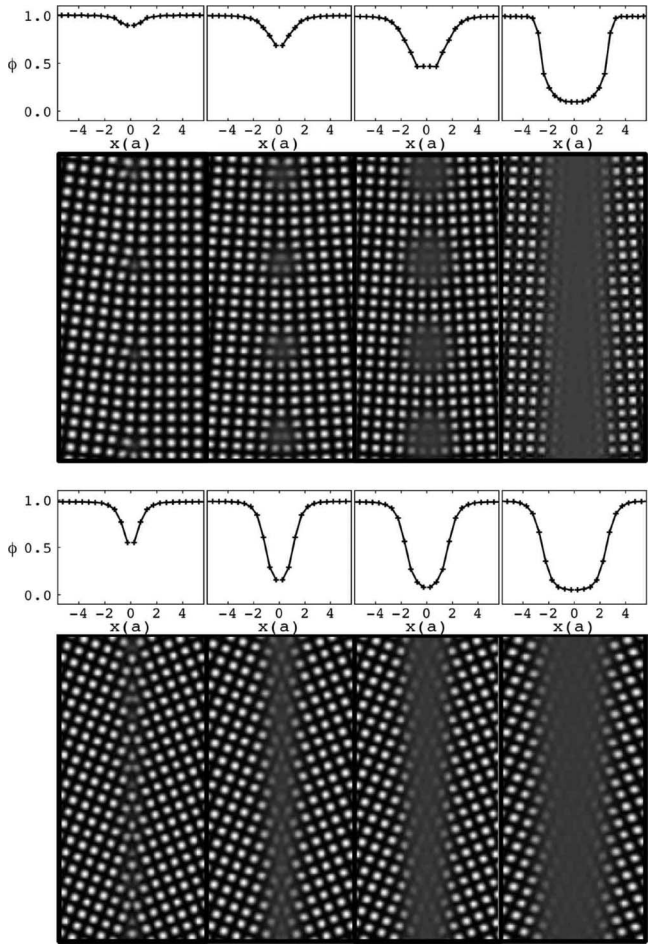

FIG. 2. Laterally averaged crystallinity parameter ϕ and cross sections of the time-averaged number density field $n(x,y,z)$ for 8° (upper) and 44° (lower) grain boundaries. ΔB=0.021 65, 0.026 27, 0.026 56, and 0.026 85 and ΔB=0.024 25, 0.024 68, 0.025 40, and 0.026 56 from left to right, respectively.

the shear modulus. For a screw dislocation $\alpha_s = b^2/4\pi^2$ and for an edge dislocation $\alpha_e = \alpha_s/(1-\sigma)$, where σ is the Poisson ratio. If we assume this result to hold for an isolated dislocation in the PFC model, at distances approaching the core region, then R_m can be directly calculated by determining the distance at which $\bar{F}_{\rm el}$ is sufficiently large to destabilize the crystalline phase, melting the dislocation core.

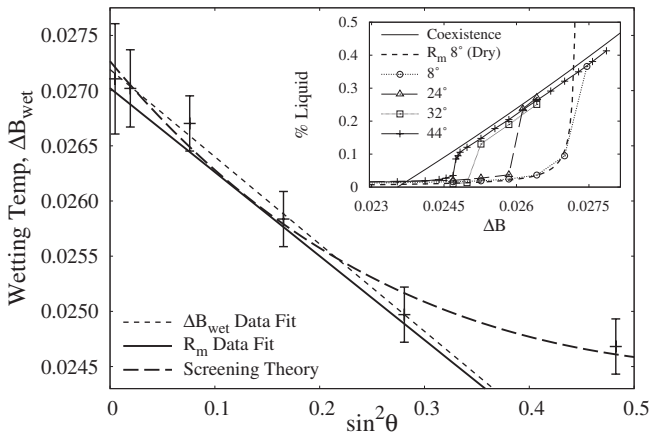

FIG. 3. Grain-boundary wetting temperature vs $\sin^2\theta$. The fit lines are discussed in the text. Inset: liquid volume fraction vs ΔB for various grain boundaries. The dashed line corresponds to the liquid volume fraction predicted for the 8° boundary based on Eq. (6) only (ignoring coexistence).

It will be assumed that n can be represented in a one mode approximation for a bcc lattice, i.e., $n(\vec{r}) = A(\cos qx \cos qy + \cos qx \cos qz + \cos qy \cos qz)$. Substituting n into Eq. (1) and minimizing with respect to q gives

$$\Delta f^X = \frac{3}{8}\Delta B A^2 - \frac{w}{8}A^3 + \frac{45}{256}A^4, \tag{4}$$

where $\Delta f^X \equiv (F - F_L)/V$, F_L is the free energy of the liquid, $V=(2\pi/q)^3$, and $q_{\rm min}=\sqrt{2}/2$. The shear modulus can be estimated in the one mode approximation by setting $n(x,y,z) \rightarrow n(x+\zeta y, y, z)$ and expanding F in ζ such that $F=F(\zeta=0) + \mu\zeta^2 + \cdots$. This procedure gives $\mu/k_BTL^2\bar{\rho} = A^2B_s/8$. The total (dimensionless) free energy of the system with a dislocation is then $\Delta f^X + \bar{F}_{\rm el}/k_BT\bar{\rho}L^d$, which can be written as

$$\Delta f = \frac{3}{8}\left(\Delta B + \frac{E}{\bar{R}^2}\right)A^2 - \frac{w}{8}A^3 + \frac{45}{256}A^4, \tag{5}$$

where $E_s \equiv B_s/(12\pi^2)$ and $E_e \equiv E_s/(1-\sigma)$ for screw and edge dislocations, respectively, and $\bar{R} \equiv R/b$. Equation (5) indicates that the elastic energy "shifts" the effective temperature ΔB by an amount $E/\bar{R}^2$. The implication is that the liquid-solid transition is shifted and instead of occurring when $\Delta B = \Delta B_m$ occurs when $\Delta B + E/\bar{R}^2 = \Delta B_m$. Thus the premelt radius can be written as

$$\bar{R}_m = \sqrt{E/(\Delta B_m - \Delta B)} \tag{6}$$

or $1/\bar{R}_m^2 = (\Delta B_m - \Delta B)/E$. A more detailed analysis considering the global F condition for melting, rather than this local condition, gives essentially the same result in the limit of zero liquid-solid surface tension.

As shown in Fig. 1, this form is consistent with the simulation results for edge dislocation pairs, though the predicted slope $(-1/E_e)$ is smaller in magnitude by a factor of nearly 5. A more definitive test would require additional data very near ΔB_m, a region increasingly difficult to access due to system size requirements. The primary source of error in the slope is likely to be overestimation of the strain energy very near the core or premelt radius in the linear elastic approximation, which directly reduces the magnitude of the slope $-1/E_e$. Additional strain energy, independent of the dislocation energy, may also be generated if the cylinder of liquid and the surrounding crystalline matrix have differing densities, an effect neglected in our calculations. This Eshelby strain energy varies as $1/R^2$ and can therefore be absorbed into the prefactor E, though our findings suggest that its contribution is relatively small.

Low angle boundaries

This description for isolated dislocations can be extended to low angle grain boundaries since an isolated dislocation is

simply the $d \to \infty$ or $\theta \to 0$ limit of a grain boundary. For $\theta \lesssim 5° - 10°$ the stress and strain fields of the individual dislocations within the boundary can be shown to be modified only slightly near their cores when the superposition of fields due to all other dislocations in the array is carried out. Therefore one may reasonably expect the melting behavior of dislocations within low angle grain boundaries to be well approximated by the isolated dislocation limit. Exploiting this fact, we can proceed to estimate the grain-boundary wetting temperature ΔB_{wet} where neighboring dislocations coalesce in low angle boundaries by setting $\bar{R}_m = d/2 = 1/(2 \sin \theta)$. Substituting Eq. (6) for $\bar{R}_m$ gives

$$\Delta B_{\text{wet}} = \Delta B_m - 4E \sin^2 \theta, \tag{7}$$

which is in good agreement with the data shown in Fig. 3. As $\theta \to \theta_{\max}$ this approximation loses validity due to the gradual deviation of the dislocation energies from the isolated dislocation result. The observed agreement up to $\theta \simeq 32°$ is somewhat unexpected as the superposition generally loses accuracy for $\theta \gtrsim 10°$. The best fit line predicts $\Delta B_m = 0.0272$, again near the measured value.

The solid line in Fig. 3 corresponds to the fit line from Fig. 1 set equal to $1/(2 \sin \theta)$ and solved for ΔB_{wet}. The agreement here clearly indicates that the wetting of low angle and intermediate angle grain boundaries is accurately described by the coalesence of radially melted regions around nearly isolated dislocations.

High angle boundaries

In the limit of large θ $(d \to 0)$, the grain-boundary energy becomes increasingly uniform along its length (see Fig. 2) and can no longer be described linearly in terms of individual dislocations. We expect that elastic fields at long distances are screened by closely spaced "dislocations," giving rise to exponentially decaying spatial grain-boundary energy. Indeed, direct analysis of free-energy data from simulations indicates that such an exponential form is qualitatively correct. Solving for ΔB_{wet} using $\bar{F}_{\text{el}} \propto f_1(\theta) e^{-\bar{R} f_2(\theta)} / \bar{R}^2$ rather than $\bar{F}_{\text{el}} \propto 1/\bar{R}^2$ gives $\Delta B_m - \Delta B_{\text{wet}} \propto f_1(\theta) e^{-f_2(\theta)}$. This is the form of the wide dashed line in Fig. 3 when $f_1(\theta) \propto \sin^2 \theta$ and $f_2(\theta) \propto \sin^2 \theta$, which more accurately captures the behavior for large θ.

IV. COEXISTENCE AND THE CANONICAL ENSEMBLE

Some comments concerning the influence of liquid-solid coexistence and the canonical ensemble (i.e., conserved density) on grain-boundary melting may be helpful at this point. The equilibrium state for a simple system with a grain boundary is most generally either dry if $F_{\text{gb}} < 2F_{\text{ls}} + \ell(\bar{F}_L - \bar{F}_X)$ or wet if $F_{\text{gb}} > 2F_{\text{ls}} + \ell(\bar{F}_L - \bar{F}_X)$, where F_{gb} is the grain-boundary energy, F_{ls} is the energy of a liquid-solid interface, and ℓ is the width of the liquid region in the wet state. If the wet state becomes favorable below the melting temperature, then a grain-boundary wetting transition occurs. In the canonical ensemble as examined here, the effects of liquid-solid coexistence and the subsequent shifts in density of the two phases above the solidus ΔB_{sol} modify this heuristic argument. Now ΔB_m, the temperature at which $\bar{F}_L = \bar{F}_X$, is straddled by a coexistence region. As $\Delta B \to \Delta B_m$ the system first encounters a solidus above which some volume fraction of liquid will minimize the overall $\bar{F}$. For the grain-boundary pair geometry, the equilibrium state above ΔB_{sol} is one with a uniform volume of liquid occupying each boundary region. Therefore, an equilibrium first-order wetting transition will occur at ΔB_{sol} as long as the grain size is not excessively small. Above ΔB_{sol}, the liquid layer width will be controlled by coexistence rather than local defect energies, since the elastic fields of the grains largely decouple $(\bar{F}_{\text{el}} \to 0)$ upon wetting.

The results presented here show no wetting or strong premelting for $\Delta B \leq \Delta B_{\text{sol}}$, and the equilibrium wetting transition is not observed. Instead, a θ-dependent discontinuous transition from the metastable dry boundary state to the equilibrium wet state occurs at $\Delta B_{\text{sol}} < \Delta B_{\text{wet}} < \Delta B_m$, as shown in the inset of Fig. 3. This is because the wetted state is not nucleated in observable times until R_m has grown sufficiently large to coalesce and the free-energy barrier approaches zero. The dislocations and/or grain boundaries act as nucleation sites for the liquid above ΔB_{sol}, creating well-defined nonequilibrium paths from the metastable dry state to the F minimizing wet state (which all must conserve ρ).

The condition for wetting in the canonical ensemble involves the grain size L_g, such that wetting can be suppressed to temperatures above ΔB_{sol} when L_g is finite. The condition can be written as $F_{\text{gb}} + L_g \Delta F_X > 2F_{\text{ls}} + \ell \Delta F_C$, where $\Delta F_X = \bar{F}_X[\bar{\rho}] - \bar{F}_X[\rho_X]$ and $\Delta F_C = \bar{F}_L[\rho_L] - \bar{F}_X[\rho_X]$. Here $\ell = (\rho_X - \bar{\rho})/(\rho_X - \rho_L)$, $\bar{\rho}$ is the conserved system density, and ρ_X and ρ_L are the shifted coexistence densities of the solid and liquid phases, respectively. For $\Delta B \leq \Delta B_{\text{sol}}$, if we assume that $\Delta F_X = 0$ and $\rho_L = \rho_X = \bar{\rho}$ (this is not the case when premelting is strong below ΔB_{sol}), we recover the original inequality $F_{\text{gb}} > 2F_{\text{ls}} + \ell(\bar{F}_L - \bar{F}_X)$ and L_g is not a significant factor. In the limit $L_g \to \infty$, the wetting condition will always be satisfied for $\Delta B > \Delta B_{\text{sol}}$ and the equilibrium transition occurs at ΔB_{sol}. As L_g decreases, the equilibrium wetting transition is shifted to higher ΔB.

V. GRAND CANONICAL ENSEMBLE

Three-dimensional simulations have also been conducted in the grand canonical ensemble, i.e., nonconserved density, where the complications due to liquid-solid coexistence are avoided. In this scenario the dynamics are given by

$$\frac{\partial n}{\partial t} = -\left(\frac{\delta F}{\delta n} + \mu_0 \right) + \nu, \tag{8}$$

where $\langle \nu(\vec{r}_1, t_1) \nu(\vec{r}_2, t_2) \rangle = M \delta(\vec{r}_1 - \vec{r}_2) \delta(t_1 - t_2)$. As the average chemical potential μ_0 is increased, rather than temperature, we find in general for the parameter values chosen that the equilibrium behavior for fixed grain boundaries of all angles is to remain essentially dry up to the melting point μ_0^*, above which the free energy is minimized by complete melting of the solid. This corresponds to a very weakly increasing

grain-boundary width and discontinuous melting at μ_0^*. The energy barrier to melt the crystal is sufficiently large that considerable superheating is instead observed in the simulations.

The melting behavior at grain boundaries is also influenced by whether the equilibrium bulk melting transition is weakly or strongly first order. For large w the bulk melting transition is strongly first order and the energy of a liquid-solid interface is prohibitively large to allow any boundary wetting below μ_0^*. Thus the grain-boundary melting transition is also strongly discontinuous. As w is lowered and the bulk transition becomes more weakly first order, both the grain boundary and the liquid-solid interface become increasingly diffuse or "soft," as shown in Fig. 4. This allows greater growth in the width of the grain boundary and potentially a weak divergence in width very near μ_0^* before complete melting occurs. Thus, a more weakly discontinuous grain-boundary melting transition is observed. This diverging width for small w may reflect increasing delocalization of the "soft" solid phase rather than the emergence of a fully liquid layer.

It is also apparent from the simulations that many states from dry to varying degrees of wet become metastable for long times near μ_0^*, such as those shown in Fig. 4. The states obtained near the melting point may therefore depend on the initial state of the system and the waiting time and may not correspond to the state of lowest free energy. In our simulations, the dry states were found to have lowest free energy up to μ_0^* for all parameter values examined.

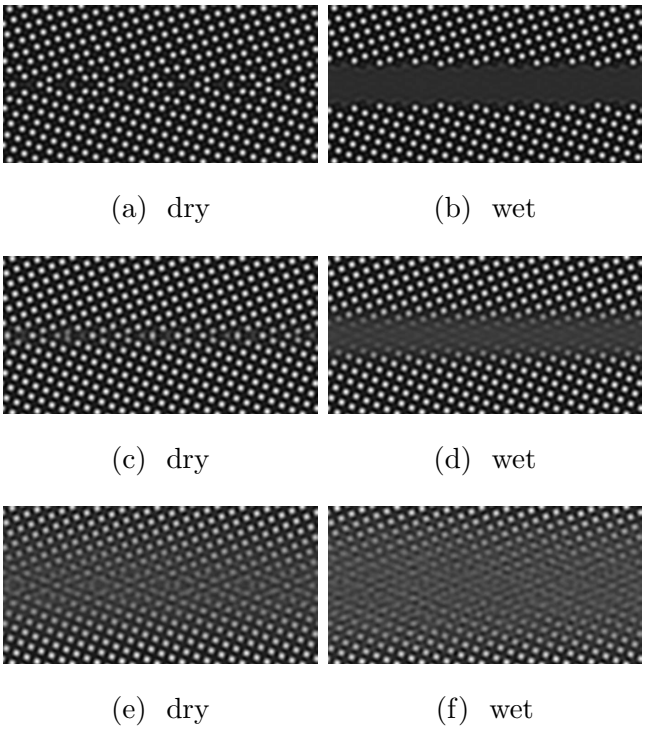

FIG. 4. Cross sections of the time-averaged number density field $n(x,y,z)$ for dry and wet 44° grain boundaries simulated with nonconserved density. The images illustrate the increase in boundary/interface diffuseness and loss of distinction between wet and dry states as the transition becomes more weakly first order. [(a) and (b)] $w=1.167$, $\Delta B=0.051\,82$, and $\mu_0=0.175\,85$, [(c) and (d)] $w=0.658$, $\Delta B=0.027\,42$, and $\mu_0=0.063\,39$, and [(e) and (f)] $w=0.174$, $\Delta B=0.001\,77$, and $\mu_0=0.015\,96$.

ACKNOWLEDGMENTS

J.B. would like to acknowledge support from the Richard H. Tomlinson and Carl Reinhardt Foundations of McGill University and thank Maria Kilfoil, Dan Vernon, Zhi-Feng Huang, Katsuyo Thornton, and Nilima Nigam for useful discussions. K.R.E. acknowledges support from the National Science Foundation under Grant No. DMR-0413062. M.G. acknowledges support from the Natural Sciences and Engineering Research Council of Canada and le Fonds québécois de la recherche sur la nature et les technologies.

[1] D. W. Oxtoby, Nature (London) **347**, 725 (1990).
[2] H. Löwen, Phys. Rep. **237**, 249 (1994).
[3] A. M. Alsayed *et al.*, Science **309**, 1207 (2005).
[4] T. Hsieh and R. Balluffi, Acta Metall. **37**, 1637 (1989).
[5] E. Budke *et al.*, Acta Mater. **47**, 385 (1999).
[6] S. Divinski *et al.*, Phys. Rev. B **71**, 104104 (2005).
[7] D. W. Demianczuk and K. T. Aust, Acta Metall. **23**, 1149 (1975).
[8] T. Watanabe *et al.*, Philos. Mag. A **49**, 845 (1984).
[9] T. Nguyen *et al.*, Phys. Rev. B **46**, 6050 (1992).
[10] J. Q. Broughton and G. H. Gilmer, Phys. Rev. Lett. **56**, 2692 (1986).
[11] R. Kikuchi and J. W. Cahn, Phys. Rev. B **21**, 1893 (1980).
[12] M. Tang *et al.*, Phys. Rev. B **73**, 024102 (2006).
[13] A. E. Lobkovsky and J. A. Warren, Physica D **164**, 202 (2002).
[14] M. Rappaz *et al.*, Metall. Mater. Trans. A **33A**, 1 (2002).
[15] K. R. Elder and M. Grant, Phys. Rev. E **70**, 051605 (2004).
[16] K. R. Elder *et al.*, Phys. Rev. B **75**, 064107 (2007).
[17] T. V. Ramakrishnan and M. Yussouff, Phys. Rev. B **19**, 2775 (1979).
[18] Y. Singh, Phys. Rep. **207**, 351 (1991).
[19] R. Ohnesorge *et al.*, Phys. Rev. E **50**, 4801 (1994).
[20] M. E. Glicksman and C. L. Vold, Surf. Sci. **31**, 50 (1972).
[21] P. M. Chaikin and T. C. Lubensky, *Principles of Condensed Matter Physics* (Cambridge University Press, Cambridge, UK, 1995).